Barrier inhomogeneities at Schottky contacts

Jürgen H. Werner and Herbert H. Güttler
Max-Planck-Institut für Festkörperforschung, Heisenbergstrasse 1, D-7000 Stuttgart 80, Federal Republic of Germany

(Received 22 August 1990; accepted for publication 26 September 1990)

We present a new analytical potential fluctuations model for the interpretation of current/voltage and capacitance/voltage measurements on spatially inhomogeneous Schottky contacts. A new evaluation schema of current and capacitance barriers permits a quantitative analysis of spatially distributed Schottky barriers. In addition, our analysis shows also that the ideality coefficient n of abrupt Schottky contacts reflects the deformation of the barrier distribution under applied bias; a general temperature dependence for the ideality n is predicted. Our model offers a solution for the so-called T_0 problem. Not only our own measurements on PtSi/Si diodes, but also previously published ideality data for Schottky diodes on Si, GaAs, and InP agree with our theory.

I. INTRODUCTION

The density j of a current $I = jF_j$ across a Schottky contact, as shown in Fig. 1, with band bending V_d and barrier height Φ_b under bias U on a moderately doped semiconductor is usually described within the thermionic emission theory:[1]

$$j = j_0 (e^{qU/(nkT)} - 1), \tag{1a}$$

$$j_0 = A^* T^2 e^{-q\Phi_{b0}^j/(kT)}. \tag{1b}$$

Here F_j denotes the area which is effective for current transport, A^* is the effective Richardson constant, q is the elementary charge, k is the Boltzmann constant, T is the temperature, and n is an empirical "ideality" coefficient which should be $n = 1$ for an ideal contact. The zero-bias Schottky barrier Φ_{b0}^j is derivable from the density j_0 of the saturation current $I_0 = j_0 F_j$ with the help of a semilogarithmic current/voltage plot by extrapolating the I/U curve from a regime $qU/(nkT) \gg 1$ toward $U = 0$;[1,2] series resistances can be eliminated with an appropriate evaluation scheme.[3] The barrier Φ_{b0}^j stems therefore not from *direct* measurements of j_0, but from extrapolating the I/U curve from a regime $U > 0$ toward $U = 0$. Results for Φ_{b0}^j are consequently unsatisfactory without a quantitative physical model for the appearance of idealities $n > 1$ which control the forward-bias I/U curve of Schottky contacts.

Idealities $n > 1$ have been ascribed to several effects: (i) interface states at a thin oxide between the metal and the semiconductor,[4-7] (ii) tunneling currents in highly doped semiconductors,[8] (iii) image force lowering of the Schottky barrier in the electric field at the interface,[9] and (iv) generation/recombination currents within the space-charge region.[10] These four models describe extreme cases of Schottky contacts (interfacial layers, high doping, large fields, traps in the space-charge region), and all of them have in common that they *tacitly* assume a spatially homogeneous, more or less atomically flat interface between the metal and semiconductor; a band diagram as in Fig. 1 is presumed for the evaluation of experimental data.

The present contribution demonstrates that idealities $n > 1$ in I/U curves of abrupt Schottky contacts without interfacial layers between the metal and a moderately doped semiconductor are the result of spatial *inhomogeneities* at the metal/semiconductor interface. Our analytical model explains not only values $n > 1$, but also their temperature dependence and the different results for the Schottky barriers from current/voltage (I/U) and capacitance/voltage (C/U) measurements; these differences contain quantitative information about the distribution of barriers within the interface plane. The temperature dependence of the Schottky barriers Φ_{b0}^j from I/U curves as well as the curved behavior of Richardson plots is also explained by our model of potential fluctuations. The ideality n is the result of the *deformation* of the spatial barrier distribution when a bias voltage is applied. Recently, we demonstrated that noise properties of Schottky diodes and grain boundaries are also correlated with spatial inhomogeneities.[11,12]

This paper is organized as follows: Section II contains our experimental results for PtSi/Si diodes for the temperature-dependent barrier and ideality data. Section III shows that these measured data cannot be understood within con-

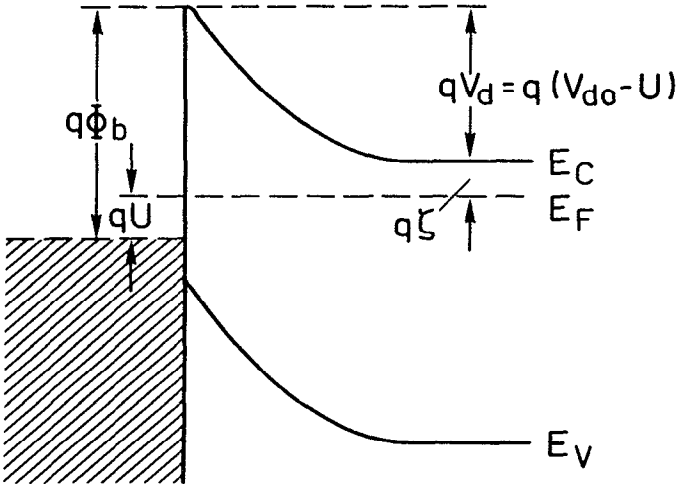

FIG. 1. One-dimensional band diagram of a Schottky diode with barrier Φ_b and band bending V_d under bias U. The quantity V_{d0} denotes the equilibrium band bending; the symbol ζ denotes the Fermi-level position in the bulk semiconductor.

 0021-8979/91/031522-12$03.00

ventional one-dimensional models for current transport across Schottky contacts. Section IV presents our model of spatial inhomogeneities, introduces effective Schottky barriers for current and capacitance measurements, and uses then the PtSi/Si data in order to exemplify the evaluation on the basis of our potential fluctuations model. Finally, Sec. V demonstrates that not only our own data, but also previously published ideality data for Schottky diodes on Si, GaAs, and InP are consistent with the predictions of our model. Our model offers a solution for the so-called T_0 problem of Schottky contacts. We reveal that the mysterious T_0, which has previously been used to fit current/voltage curves of Schottky diodes, represents the deformation of the barrier distribution upon the application of bias voltage.

II. EXPERIMENTAL RESULTS

Figure 2 shows a set of temperature-dependent current/voltage curves taken from a PtSi/Si diode No. 1 with a circular area of $F = 8.5 \times 10^{-3}$ cm^2. This diode No. 1 is prepared by evaporating 100 nm of Pt on a (100)Si wafer with a phosphorous doping $N_d = 2 \times 10^{15}$ cm^{-3}; the wafer has an implanted ohmic back-side contact with an Al metallization. The formation of the PtSi is performed by annealing at 400 °C for 20 min in a furnace under argon atmosphere. Temperature-dependent measurements are accomplished in darkness in a commercially available Oxford CF204 He cryostat. We use here the experimental data from PtSi/Si diodes in order to exemplify our model of potential fluctuations; we obtain similar results by analyzing measurements on polycrystalline Pd_2Si/Si, IrSi/Si, and $CoSi_2$/Si contacts.

Figure 3 presents a so-called Richardson plot of $\ln(j_0/T^2)$ versus inverse temperature T^{-1} for the saturation currents densities $j_0 = I_0/F$, deduced from the I/U data in Fig. 2 by extrapolating the curves toward $U = 0$. Also shown are data from a second PtSi/Si diode (PtSi/Si No. 2) with a square area of $F = 1.0 \times 10^{-2}$ cm^2. For the determination of j_0, we apply a novel evaluation scheme which makes use of the conductance $G = dI/dU$ and allows us to eliminate the series resistance of the Si substrate.[3] Plots like those

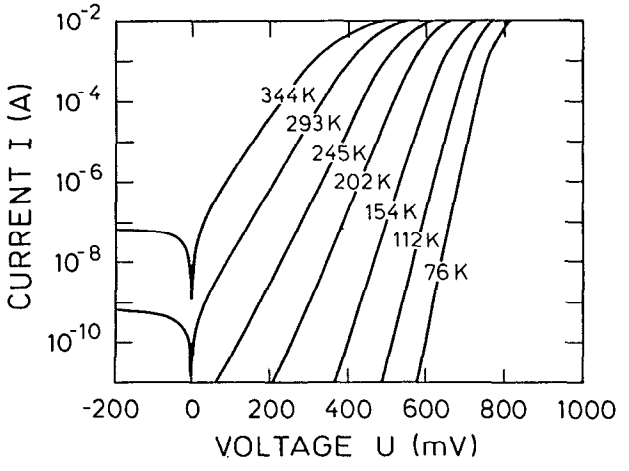

FIG. 2. Current/voltage curves of PtSi/Si diode No. 1. All these curves can be fitted with an ideality n, which is independent of bias voltage U, but depends on temperature T.

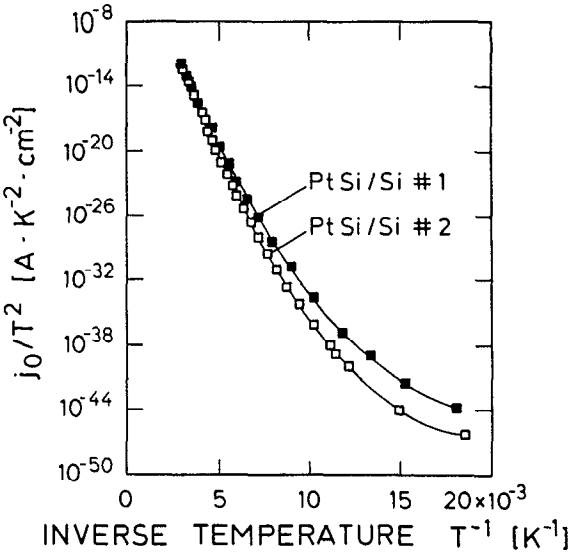

FIG. 3. Richardson plot of the saturation currents j_0 which are obtained from the I/U curves in Fig. 2 with the help of Eq. (1a). Data for a second diode (PtSi/Si No. 2) are also shown. The plots are curved because the Schottky barriers Φ_{b0} depend on temperature T as shown in Fig. 4.

in Fig. 3 are often used to determine the Schottky barrier from the slope of the anticipated thermally activated behavior:[2,3] According to Eq. (1b), one obtains

$$\ln(j_0/T^2) = \ln(A^*) - \frac{q\Phi^j_{b0}}{kT}, \tag{2a}$$

$$E_{act} := k\frac{d[\ln(j_0/T^2)]}{d(1/T)} = -q\Phi^j_{b0}, \tag{2b}$$

and the plot in Fig. 3 therefore should yield a straight line with an activation energy E_{act} if the Schottky barrier Φ^j_{b0} is independent of temperature T. The bowing of the curve in Fig. 3 demonstrates that it is impossible to fit our data with a temperature-*independent* barrier Φ^j_{b0}. Therefore, we determine $\Phi^j_{b0}(T)$ directly from the j_0 values with the help of Eq. (1b) and a Richardson constant $A^* = 112$ A/cm^2 K^2, which is typical for n-type Si.[13] Results for $\Phi^j_{b0}(T)$ are shown in Fig. 4 together with values for the temperature-dependent ideality $n(T)$. We find that our I/U curves are well described by Eq. (1) with an ideality n which is independent of voltage U, but depends on temperature T.

Figure 4 compares the current-barrier Φ^j_{b0}-to-$\Phi^{C'}_{b0}$ data, which are obtained from the evaluation of the extrapolated flatband voltage U_f of reverse-bias capacitance/voltage curves as in Fig. 5. These C/U data are independent of frequency between 1 kHz and 1 MHz. This finding indicates that our diodes do not contain a measurable amount of deep levels within the space-charge region and that the influence of minority carriers on current transport can be neglected.[4,6] The only contribution to the capacitance C thus stems from the displacement current within the space-charge region.[4] If we use a one-dimensional description for the evaluation of measured capacitances C, one can write[1,2]

$$C_F = \chi(V_d - kT/q)^{-1/2}, \tag{3a}$$

with the abbreviation

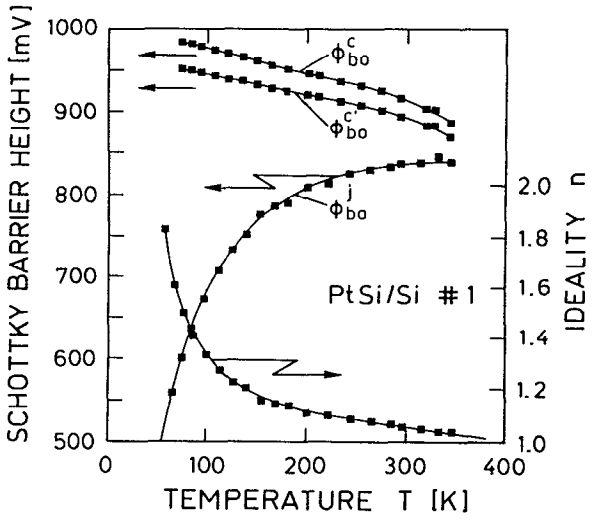

FIG. 4. The (zero-bias) current barrier Φ_{b0}^{j} and ideality n from I/U measurements and the capacitance barrier $\Phi_{b0}^{C'}$ from C/U data depend on temperature T. The differences between current and capacitance barriers are the result of spatial potential fluctuations. The Φ_{b0}^{C} data represent the *zero-bias* capacitance barrier after correcting the $\Phi_{b0}^{C'}$ data for a linear voltage dependence of the mean Schottky barrier $\bar{\Phi}_b$.

$$\chi = (q\epsilon_s N_d/2)^{1/2}, \tag{3b}$$

for the areal space-charge capacitance $C_F = C/F_C$. Here F_C denotes the area which is effective for capacitances and ϵ_s is the semiconductor's dielectric constant. The diffusion potential V_d depends on voltage U according to $V_d = V_{d0} - U$ with the zero-bias value V_{d0}. The extrapolated zero-bias built-in potential $V_{d0}^{C'}$ can therefore be determined from the flatband voltage U_f in Fig. 5 for which $1/C^2 = 0$ holds, according to

$$C_F^{-2} = \chi^{-2}(V_{d0}^{C'} - U - kT/q), \tag{3c}$$

and

$$V_{d0}^{C'} = U_f + kT/q. \tag{3d}$$

The Schottky barrier $q\Phi_{b0}^{C'}$ follows from

$$\Phi_{b0}^{C'} = V_{d0}^{C'} + \zeta = U_f + kT/q + \zeta. \tag{3e}$$

The superscript C' stands for the fact that the data have been derived from $1/C^2$ plots assuming a one-dimensional model for a Schottky barrier $\Phi_{b0}^{C'}$ which is independent of voltage U (see Sec. IV E). The semiconductor Fermi level $q\zeta = kT\ln(N_C/N_d)$ in Eq. (3e) depends on the effective density of states N_c in the conduction band and on the doping N_d, which is deducible from the slope of the $1/C^2$ plot according to

$$\frac{d(C_F^{-2})}{dU} = \frac{-2}{q\epsilon_s N_d}. \tag{3f}$$

Figure 4 reveals a drastic difference between the barriers $\Phi_{b0}^{C'}$ and Φ_{b0}^{j}, which are derived from capacitance C and dc current I; for all temperatures we find $\Phi_{b0}^{j} < \Phi_{b0}^{C'}$. The room-temperature values for sample No. 1 are $\Phi_{b0}^{j} = 837$ mV and $\Phi_{b0}^{C'} = 892$ mV. In the following we show that such differences in Fig. 4, the curved behavior of the Richardson plot in Fig. 3, as well as the temperature dependence of the idealities $n > 1$ cannot be understood within conventional models which are based on the assumption of spatially homogeneous diodes. Instead, all our experimental findings are quantitatively described by our new model of potential fluctuations for spatial inhomogeneities within the interface plane of Schottky contacts.

III. COMPARISON WITH ONE-DIMENSIONAL MODELS

Interfacial oxides do not occur at our abrupt silicide/Si Schottky contacts; therefore, they cannot be made responsible for the observed idealities $n > 1$. Forward-bias ac admittances $Y = G + i\omega C$ do not yield any frequency dispersion for the conductance G and the capacitance C between 5 Hz and 10 MHz; the ac conductance G equals the slope of the dc I/U curve, and the capacitances C always equal the displacement current within the space-charge region. Models which ascribe the ideality $n > 1$ to interface states[4–6] or insulating layers at the interface are therefore inappropriate to explain $n > 1$ and the temperature dependence of n in Fig. 4. In addition, the different results for the Schottky barriers from I/U and C/U experiments as well as the temperature dependencies of these quantities are hard to understand within these theories.[4–6]

Tunneling through the top of the Schottky barrier could in principle be a reason for the I/U barrier Φ_{b0}^{j} being smaller than the C/U barrier $\Phi_{b0}^{C'}$ and for idealities $n > 1$. Capacitances C are insensitive to tunneling, whereas I/U curves measure a lower barrier. However, the expected barrier decrease is too small to explain our experimental results: The characteristic tunneling energy E_{00} of Padovani and Stratton,[14]

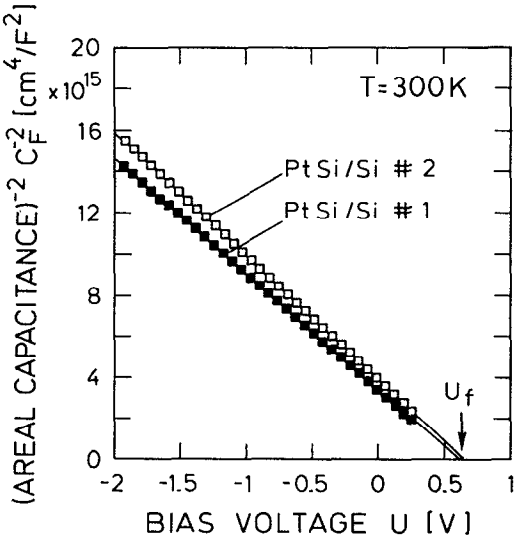

FIG. 5. The evaluation of capacitance/voltage plots yields the flatband voltage U_f. The capacitance barriers $\Phi_{b0}^{C'}$ are then obtained from Eq. (3e) (for a one-dimensional model) or from Eq. (26a) (for our potential fluctuation model).

$$E_{00} = \frac{\hbar}{2}\sqrt{\frac{N_d}{m^*\epsilon_s}}, \tag{4a}$$

amounts to 0.42 meV for our moderately doped Si substrates. The effective tunneling barrier lowering

$$\Delta\Phi_{tunn} = (1.5E_{00})^{2/3}V_d^{1/3} \tag{4b}$$

equals 6.8 meV for $qV_d = 0.8$ eV and is therefore much smaller than the several hundred meV barrier difference in Fig. 4 which we observe between C/U and I/U barriers; in addition, our measured barrier differences are temperature dependent, whereas results from Eq. (4b) are independent of T. On the other hand, the ideality n_{tunn} for tunneling should be temperature dependent according to[8]

$$n_{tunn} = \frac{qE_{00}}{kT}\coth\left(\frac{qE_{00}}{kT}\right), \tag{4c}$$

which predicts $n_{tunn} = 1.000\,08$ at 300 K and $n_{tunn} = 1.001\,31$ at 77 K for our moderately doped Si. These values are much too low to explain our measured $n = 1.05$ at 300 K and $n = 1.5$ at 77 K for PtSi No. 1. Doping densities above 3×10^{16} and 1×10^{18} cm^{-3} at 300 and 77 K, respectively, are necessary in order to cause $n > 1.05$ by tunneling across Schottky diodes on Si. Tunnel currents therefore do not explain the barrier differences and ideality data in Fig. 4.

Models[9,15,16] for *image force lowering* also fail to explain our experiments: Image forces alone yield a (positive) barrier lowering with respect to the flatband of[16]

$$\Delta\Phi_{imf} = \sqrt{\frac{qE_{max}}{4\pi\epsilon_s}}. \tag{5}$$

For a (zero-bias) Schottky barrier height of 850 mV on our Si with a doping $N_d = 2\times10^{15}$ cm^{-3}, Eq. (5) yields for $T = 300$ K a value of $\Delta\Phi_{imf} \approx 15$ mV with a maximum electric (zero-bias) field $E_{max} = 1.47\times10^4$ V/cm; for $T = 77$ K and $E_{max} = 2.19\times10^4$ V/cm we obtain $\Delta\Phi_{imf} \approx 16.2$ mV. The ideality n_{imf} due to image force lowering follows from Eq. (3.14) of Ref. 16. For a typical bias voltage $U = 0.4$ V, we obtain $n_{imf} = 1.038$ for 300 K and $n_{imf} = 1.042$ for 77 K; these values are again too low to explain our measured n data. If one considers also quantum-mechanical reflection and tunneling *in addition* to image force lowering, then according to Chang and Sze[15] one would expect an increase of the ideality n with decreasing temperature. However, the value[15] $n_{imf,tunn} = 1.09$ at 77 K, which one expects for our Si doping due to all these combined effects, is again too low to explain the data in Fig. 4.

Generation(G)/recombination(R) currents in the space-charge region (i.e., simultaneous emission/capture of electrons and holes at deep traps) seem also inappropriate to explain our experimental barrier and ideality data. First, the absence of a frequency-dependent capacitance and conductance under *forward* bias indicates that minority carriers—which could be detected due to their diffusion capacitance—play (if at all) only a minor role in current transport.[4] Second, the complete absence of a frequency dependence in the admittance under *reverse* bias demonstrates that the space-charge region is free of deep levels which could be made responsible for minority-carrier recombination. Third, the I/U curves in Fig. 1 are also too smooth to explain the ideality data with such G/R currents; they should cause an additional current component which outstrips the majority-carrier current at small voltages as shown by McLean, Dharmadasa, and Williams.[17] Fourth, G/R currents could hardly explain the difference between I/U and C/U Schottky barriers.

At last, we can also exclude the possibility that the different barriers from I/U and C/U data and their temperature dependencies as well as of the ideality n could result from any currents which flow over the edges of our Schottky diodes. In a careful study on diodes with different areas, we do not detect any area (and shape) dependence of the results in Fig. 4. For the evaluation of I/U and C/U curves, we assume therefore also that the effective areas for currents (F_j) and capacitances (F_C) are equal and also equal to the geometrical area F of the metallic PtSi contact, i.e., $F_j = F_C = F$.

IV. POTENTIAL FLUCTUATIONS MODEL

We explain the different results in Fig. 4 for the Schottky barriers from I/U and C/U measurements, and the temperature dependence of Φ_{b0}^j and of $n > 1$ by local *inhomogeneities* at the Schottky contact: The interface between the metal and semiconductor is not atomically flat but rough, with the result of spatial fluctuations of the built-in voltage V_d and the Schottky barrier Φ_b as indicated by the band diagram in Fig. 6. Apart from the roughness of the interface due to thickness modulations of the metal as well as atomic steps, dislocations, and grain boundaries in the metal, these potential fluctuations may also originate from a local effective barrier lowering due to field emission at metallic

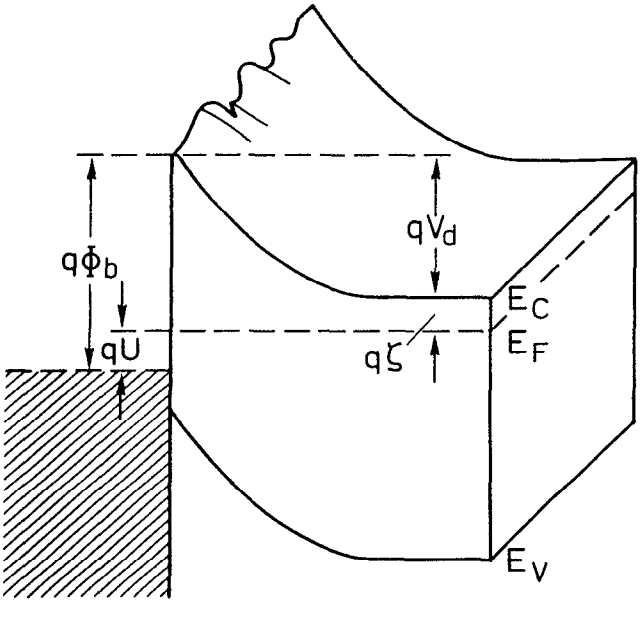

FIG. 6. Two-dimensional band diagram of an inhomogeneous Schottky contact. Spatial variations of band bending V_d and Schottky barrier Φ_b result in different Schottky barriers for currents (Φ_b^j) and capacitances (Φ_b^C). The shape and position of the ridges in the potential "mountains" depend on bias voltage and cause therefore idealities $n > 1$ in I/U curves.

diffusion spikes with narrow radii of curvature. Differences in interface metallurgy due to different metal phases generally might also be a good candidate for local variations of the effective Schottky barrier. One could also imagine that the irregular distance between the semiconductor donor atoms in the vicinity of the interface influences the potential distribution at the interface as the donors are not arranged in a regular lattice but randomly distributed. The influence of such doping fluctuations on barriers in small devices was discussed by Arnold and Hess,[18] as well as by Nixon and Davies.[19] In the present contribution we consider here *large*-area devices which contain potential fluctuations on a length scale which is *smaller* than the width of the space-charge region.

Our model of potential fluctuations differs from earlier models for inhomogeneous Schottky contacts.[20–23] The authors of these earlier publications investigated parallel connections of *discrete* and homogeneous Schottky diodes with different values of the barrier height. For example, Odomari and Tu characterized the properties of parallel connections of a network which consisted of discrete diodes of PtSi/Si and NiSi/Si.[21] They assumed that the total dc current I across the patchworklike arrangement of low-barrier NiSi/Si and high-barrier PtSi/Si Schottky contacts can be modeled by adding the low-barrier current I_l and the high-barrier current I_h linearly, i.e., $I = I_l + I_h$. Similar models were applied to interpret capacitances[21] and photoresponse measurements.[23] The effective Schottky barriers which determine currents,[20–22] capacitances,[21] and internal photoemission[23] depend then on the ratio of the areas S_l/S_h of low-barrier (S_l) and high-barrier (S_h) contacts. Similar model for current/voltage curves were published by Schneider *et al.*[24] and by Tuy and Mojzes.[25] The model of Ohdomari and Tu[20,21] explains the experimental finding that the barrier which is deduced from capacitances is higher than the one from current measurements as the dc current depends strongly on the area S_l of the low-barrier diodes. However, all these models are based on the tacit assumption that the barriers in the low- and high-barrier regimes are spatially separated and do not interact with each other; i.e., it is implicitly assumed that the fluctuations of the Schottky barrier appear on a length scale which is large compared to the widths of the space-charge regions of the well-separated high- and low-barrier regimes. Moreover, they consider only two discrete values for the barrier instead of a barrier distribution. In addition, these "patchwork" models[20–23] of discrete, noninteracting, and homogeneous diodes seem inappropriate to explain the occurrence of idealities $n > 1$ as well as the temperature dependencies of effective I/U and C/U barriers.

The limitation of spatially separated diodes was overcome by Freeouf *et al.*[26] These authors used a finite-element device analysis program (FIELDAY) and modeled the influence of size effects on the I/U and C/U curves of two contacts with overlapping and interacting space-charge regions. A low-barrier contact with $\frac{1}{8}$ of the total contact area was imbedded in a high-barrier contact of $\frac{5}{6}$ of the total contact area with a gap of $\frac{1}{24}$ in the total area; the width of the total area was varied between $\frac{1}{4}$ and 8 μm. The simulations confirmed that the effective C/U barrier is higher than the I/U barrier. The most interesting result of these studies was that the *absolute* size of the regions with the two different barriers strongly affects the conventional barrier determination from I/U and C/U curves. For example, if the low-barrier region width becomes smaller, the total effective barrier becomes larger because the potentials from the high-barrier contact reach under the low-barrier metal; the low-barrier contact is thus effectively pinched off.

The main disadvantage of all these previous models of inhomogeneous Schottky contacts is their limitation to *two* different and discrete values for the Schottky barrier.[20–26] These descriptions are either based on the assumption of discrete, spatially separated, and homogeneous barriers,[20–24] or they require numerical device modeling.[26] Our new model of potential fluctuations is free of these restrictions; it allows for an *analytical* description of the temperature-dependent transport properties of Schottky contacts with a continuous range of spatially distributed barriers.

A. Gaussian barrier distribution $P(\Phi_b)$

Our model of potential fluctuations assumes a continuous barrier distribution at the interface between the metal and semiconductor. We consider fluctuations of band bending V_d and Schottky barriers Φ_b which occur on a length scale small compared to the width of the space-charge region, i.e., < 1 μm for a moderately doped semiconductor. The model proposed here is similar to the theory[27,28] which we developed to explain electronic transport across grain boundaries. Some aspects of this earlier *analytical* model which considered the influence of potential fluctuations on dc current,[28] admittances,[27,28] and noise[12] at Si bicrystals were independently discussed by Thomson and Card.[29] In a rigorous *numerical* analysis which used idealized assumptions (as voltage-independent and mobile interface charges), Mahan elucidated later also the differences between current and capacitance barriers which arise due to statistical donor fluctuations in the vicinity of grain boundaries.[30]

The model presented here is designed to analyze transport properties of Schottky diodes; it allows not only to explain the differences of barriers which are derived from capacitances and currents, but it interprets also the meaning of idealities $n > 1$ as well as their temperature dependence. The description is analytical and does not require computer simulations.

We mimic the spatial distribution of the band bending V_d at the metal/semiconductor interface of Schottky contacts by a Gaussian distribution $P(V_d)$ with a standard deviation σ_s around a mean $\bar{V}_d$ value according to

$$P(V_d) = \frac{1}{\sigma_s\sqrt{2\pi}} e^{-(\bar{V}_d - V_d)^2/(2\sigma_s^2)}. \tag{6}$$

The band bending V_d and consequently also the Schottky barrier

$$\Phi_b = V_d + \zeta + U \tag{7}$$

depend therefore on the location within the interface plane with a barrier distribution

$$P(\Phi_b) = \frac{1}{\sigma_s\sqrt{2\pi}} e^{-(\overline{\Phi}_b - \Phi_b)^2/(2\sigma_s^2)} \tag{8}$$

around a mean Schottky barrier $\overline{\Phi}_b$. The barrier distributions are normalized:

$$\int_{-\infty}^{\infty} P(V_d)dV_d = \int_{-\infty}^{\infty} P(\Phi_b)d\Phi_b = 1. \tag{9}$$

B. Effective barriers for current *I* and capacitance *C*

The spatial distributions of potentials and barriers influence capacitance and dc current measurements differently: The capacitance C stems from the displacement current $dE/dt = i\omega C$, which in turn originates at frequency ω from the time periodic change of the width of the space-charge region. These widths depend on the mean electric field E at the metal/semiconductor interface. Short-wavelength potential fluctuations at the metal/semiconductor interface are screened out at the edge of the space-charge region. Consequently, capacitances are expected to measure only the *mean* values $\overline{V}_d$ and $\overline{\Phi}_b$; the capacitance C is insensitive to potential fluctuations on a length scale of less than the space-charge width. The dc current I across the interface depends, on the other hand, *exponentially* on Φ_b and thus sensitively on the detailed barrier distribution at the interface. Any spatial variation in the barriers causes the current I to flow preferentially through the barrier minima. One expects therefore intuitively that Schottky barrier values determined by I/U measurements are lower than those which follow from C/U data.

A quantitative expression for the effective band bending V_d^j and barrier Φ_b^j, which control the net current density $j = j_{sm} - j_{ms}$ through an inhomogeneous Schottky contact, can be derived with the help of the thermionic emission theory, similarly to a homogeneous contact. The density of the current j_{sm} from the semiconductor into the metal across the band bending V_d and the current j_{ms} from the metal in the semiconductor are written as

$$j_{sm} = A^* T^2 e^{-q\zeta/kT} e^{-qV_d/kT}, \tag{10a}$$

and

$$j_{ms} = A^* T^2 e^{-q\Phi_b/kT}. \tag{10b}$$

For a distribution $P(V_d)$ of potentials, we integrate j_{sm} over all potentials V_d, resulting in

$$j_{sm} = A^* T^2 e^{-q\zeta/kT} \int_{-\infty}^{\infty} e^{-qV_d/kT} P(V_d)dV_d. \tag{11}$$

Appendix A shows that the integration in Eq. (11) yields the effective band bending V_d^j for the current j_{sm} as

$$V_d^j = \overline{V}_d - \frac{\sigma_s^2}{2kT/q}, \tag{12}$$

allowing us to write j_{sm} in the usual form:

$$j_{sm} = A^* T^2 e^{-q\zeta/kT} e^{-qV_d^j/kT}. \tag{13}$$

A similar integration for j_{ms} in Eq. (10b) yields

$$\Phi_b^j = \overline{\Phi}_b - \frac{\sigma_s^2}{2kT/q}. \tag{14}$$

Equations (7), (10), and (14) permit us therefore to include the consequence of potential fluctuations into the usual thermionic emission theory just by writing

$$j = A^* T^2 e^{-q\Phi_b^j(U,T)/kT}(e^{qU/kT} - 1), \tag{15}$$

with an the effective current barrier Φ_b^j which obeys Eq. (14); this equation shows also that Φ_b^j is indeed always smaller than the mean barrier $\overline{\Phi}_b$.

The barrier Φ_b^C, which is effective for capacitance C, is considered in Appendix B. There it is algebraically confirmed that C depends only on the mean band bending $\overline{V}_d$ and is insensitive to the standard deviation σ_s of the barrier distribution $P(\Phi_b)$. We find $V_d^C = \overline{V}_d$ and

$$\Phi_b^C \equiv \overline{\Phi}_b; \tag{14'}$$

the capacitance barrier Φ_b^C is equal to the mean barrier $\overline{\Phi}_b$.

C. Temperature-dependent barriers

Equations (14) and (14') are the cornerstones of our model of spatial inhomogeneities; these relationships in Eqs. (14) hold for any dependence of current barriers Φ_b^j, capacitance barriers $\Phi_b^{C'}$, mean barriers $\overline{\Phi}_b$, and standard deviations σ_s on temperature T and/or bias voltage U. These equations permit us to explain the different barriers from I/U and C/U data. Moreover, we show below that consideration of the *deformation* of the barrier distribution under bias U permits to explain also the ideality n. It is therefore interesting to note that already the nontrivial assumption that the *width* of the Gaussian barrier distribution (i.e., its standard deviation σ_s) is *independent* of temperature T allows for an explanation of the temperature-dependent barrier data in Fig. 4: Under these conditions a plot of $\overline{\Phi}_b - \Phi_b^j$ vs T^{-1} should yield a straight line through the origin with a slope of $q\sigma_s^2/(2k)$.

Figure 7 shows results for our two PtSi/Si Schottky diodes; the slope of curve (a) for our sample No. 1 yields $\sigma_s(T=0) = 68.5$ mV; from curve (b), for sample No. 2, we find $\sigma_s(T=0) = 68.9$ mV. We find such a linear dependencies also for the majority of other silicide/silicon Schottky contacts. Our analytical model of barrier inhomogeneities is therefore in quantitative agreement with experiment; it explains the large barrier differences from Fig. 4 over the whole range of temperatures without any further assumptions.

Curves (a) and (c) in Fig. 7 exhibit y-axis intercepts which do not exactly equal zero as is anticipated on the basis of Eq. (14). One is attempted to ascribe this finding to a *temperature dependence* of σ_s according to

$$\sigma_s^2(T) = \sigma_s^2(T=0) + \alpha_\sigma T. \tag{16a}$$

A *linear* behavior following Eq. (16a) would still preserve a linear dependence in a delineation as in Fig. 7 with a slope $q\sigma_s^2(T=0)/2k$ and a y-axis intercept $q\alpha_\sigma/2k$. From curve (a) in Fig. 7, a fit to Eq. (16a) yields $\alpha_\sigma = -4.3\ \text{mV}^2/\text{K}$ for sample No. 1; curve (c) yields $\alpha_\sigma = -2.1\ \text{mV}^2/\text{K}$ for sample No. 2.

Assuming a linear temperature dependence of σ_s^2 as in Eq. (16a) could also be justified: An *a priori* assumption of a temperature-*independent* σ_s, i.e., $\alpha_\sigma = 0$, is nontrivial as the capacitance data in Fig. 4 demonstrate that the *mean*

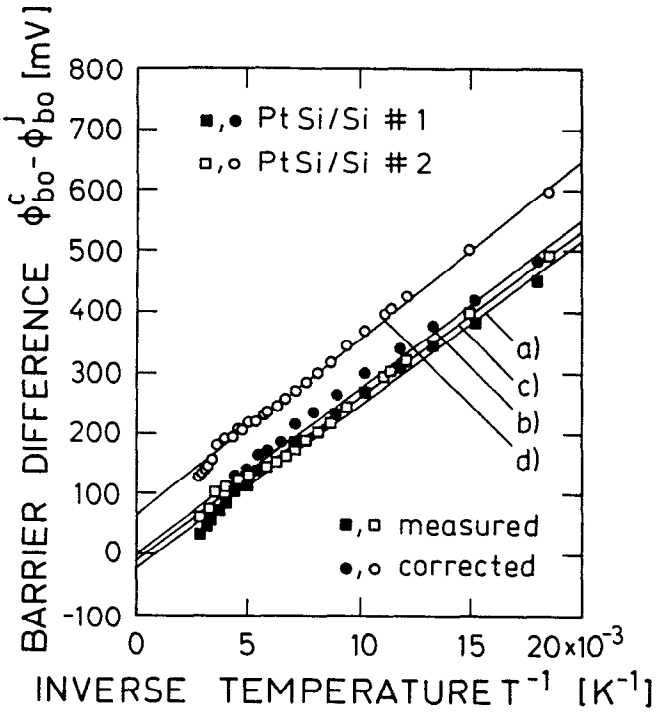

FIG. 7. Plot of differences between Schottky barriers for two PtSi/Si diodes. Curves (a) and (c) show the difference between values as derived from the conventional evaluation of I/U and C/U data. Curves (b) and (d) follow from curves (a) and (c) after correcting the capacitance barrier $\Phi_{b0}^{C'}$ for the bias dependence of the mean Schottky barrier $\overline{\Phi}_b$ according to Eq. (22a).

Schottky barrier $\overline{\Phi}_b$ itself varies also approximately linearly with T according to

$$\overline{\Phi}_b(T) = \overline{\Phi}_b(T=0) + \alpha_{\overline{\Phi}} T. \tag{16b}$$

From the $\Phi_{b0}^{C'}$ barriers in Fig. 4, we obtain $\alpha_{\overline{\Phi}}(1) = -0.252$ mV/K for sample No. 1 and $\alpha_{\overline{\Phi}}(2) = -0.326$ mV/K for sample No. 2. Within our model of potential fluctuations, the mean barrier $\overline{\Phi}_b$ resembles the role of the fundamental Schottky barrier in the commonly used *one*-dimensional Schottky barrier theories. However, the temperature dependence of our $\overline{\Phi}_b$ is much larger than the coefficients which are expected from the temperature coefficient α_{DME} of the so-called dielectric midgap energy (DME) of Cardona and Christensen.[32] From their data, we would expect that the Schottky barrier on n-type Si varies with a coefficient of $\alpha_{\Phi,\mathrm{DME}}^{n} = -0.15$ mV/K, a coefficient with an absolute value which is much smaller than the coefficients found by us. The DME model is based on band-structure considerations and bulk properties of the semiconductor alone, and it represents therefore only a rough estimate, as the detailed (crystallographic) structure of the interface is not considered.[32]

To summarize this section, we want to point out that the differences between current and capacitance barriers are understood with the help of Eq. (14). The observation of finite y-axis intercepts in Fig. 4 could be understood if we postulated a slight temperature dependence of the Gaussian barrier distribution according to Eq. (16a). However, before ascribing the y-axis intercepts in Fig. 4 to a temperature-dependent σ_s^2, the next paragraph first considers the implicit assumptions, which are used to deduce the barrier data from measured I/U and C/U curves.

D. Voltage dependencies and ideality $n(T)$

The behavior of curves (a) and (c) in Fig. 7 is closely related to the ideality $n > 1$ and the evaluation of the current and capacitance data: Equations (14) and (14') describe the relation between current and capacitance barriers for any, *but identical* voltages. Contrarily, curves (a) and (c) in Fig. 7 represent the difference of barriers which are gained by extrapolating voltage-dependent I/U and C/U measurements, assuming the validity of Eqs. (1) and (3); i.e., we plot $\Phi_{b0}^{C'}(T) - \Phi_{b0}^{j}(T)$ from Fig. 4. The barriers $\Phi_{b0}^{j}(T)$ originate from *forward*-bias I/U measurements which are extrapolated toward $U = 0$; the values $\Phi_{b0}^{C'}$ result from extrapolating *reverse*-bias capacitances towards the flatband voltage U_f. Any voltage dependence of the effective Schottky barriers for currents (Φ_b^j) and capacitances (Φ_b^C) due to a voltage dependence of the potential distribution $P(\Phi_b)$ will therefore impair a comparison of I/U and C/U barriers on the basis of Eqs. (14).[33]

A voltage dependence of the current barrier Φ_b^j is already implicitly assumed, if we fit the I/U data with the help of Eqs. (1) and an ideality $n > 1$. The ideality n hides differences between the extrapolated zero-bias barrier Φ_{b0}^{j} and the barrier $\Phi_b^j(U)$; a proper and consistent thermionic emission (and drift/diffusion) theory does not allow for any other explanation for n. (We showed already in Sec. III that the consideration of additional transport mechanisms fails to explain $n > 1$ for our diodes.) Equating Eqs. (1) and (15) yields for the ideality

$$n^{-1}(U,T) - 1 = -\frac{\Delta\Phi_b^j(U)}{U}, \tag{17a}$$

with

$$\Delta\Phi_b^j(U) = \Phi_b^j(U) - \Phi_{b0}^j. \tag{17b}$$

Idealities $n > 1$ require $\Delta\Phi_b^j > 0$; hence, the current barrier Φ_b^j *increases* with increasing U. For example, such barrier increases with U are known from image force lowering.[9,15,16] Equation (17a) demonstrates that voltage-*independent* idealities n require a *linear* increase of $\Phi_b^j(U)$ with U, i.e.,

$$\Delta\Phi_b^j(U) = \rho_1 U, \tag{18a}$$

$$n^{-1}(T) - 1 = -\rho_1, \tag{18b}$$

and a voltage coefficient $\rho_1 > 0$ which must depend on T for a temperature-dependent $n(T)$.

If one ascribes the ideality n to a voltage-dependent current barrier $\Phi_b^j(U)$, then Eq. (14) leads to the straightforward conclusion that the mean value $\overline{\Phi}_b$ and the standard deviation σ_s depend on voltage. The hills and valleys in the ridges of the ragged potential mountains (see Fig. 6) of the barrier distribution $P(\Phi(U))$ at inhomogeneous Schottky contacts therefore must change under bias! For example, we would expect the local image forces to displace the effective barrier maxima from the rough metallurgical interface between the metal and semiconductor; the effective maxima move deeper into the semiconductor when the bias voltage

increases. Each particular bias U creates therefore a different barrier distribution in planes which are approximately parallel to the interface. Intuitively, we would also expect that the barrier distribution becomes more homogeneous (i.e., a decrease of σ_s) when larger forward-bias voltages shift the maxima deeper into the semiconductor.

Instead of describing the detailed *local* deformation of an individual barrier Φ_b of a specific Gaussian distribution by a particular bias voltage U, we model the *global* effect of the bias voltage and assume here that the distributions of barriers *always* can be described by a Gaussian. However, the distributions differ for each bias voltage; we postulate therefore that Eqs. (14) hold for all bias voltages U including $U=0$ according to

$$\Phi_{b0}^{j} = \bar{\Phi}_{b0} - \frac{\sigma_{s0}^2}{2kT/q}. \tag{19a}$$

$$\Phi_b^j(U) = \bar{\Phi}_b(U) - \frac{\sigma_s^2(U)}{2kT/q}. \tag{19b}$$

Here $\bar{\Phi}_{b0}$ and σ_{s0} stand for the mean barrier and standard deviation for thermodynamic equilibrium ($U=0$), and Φ_{b0}^j denotes the corresponding current barrier. The change of Φ_b^j under bias follows from Eqs. (17b), (19a), and (19b) as

$$\Delta\Phi_b^j(U) = \Phi_b^j(U) - \Phi_{b0}^j$$

$$= \bar{\Phi}_b(U) - \bar{\Phi}_{b0} - \frac{\sigma_s^2(U) - \sigma_{s0}^2}{2kT/q} \tag{20a}$$

$$=: \Delta\bar{\Phi}_b(U) - \frac{\Delta\sigma_s^2(U)}{2kT/q}. \tag{20b}$$

The physical meaning of the ideality n is then finally obtained by combining Eqs. (20b) and (17a), with the result

$$n^{-1}(U,T) - 1 = -\frac{\Delta\bar{\Phi}_b(U)}{U} + \frac{\Delta\sigma_s^2(U)}{2kTU/q}. \tag{21}$$

Equation (21) relates the variation of the mean barrier $\bar{\Phi}_b$ and the standard deviation σ_s of the barrier distribution $P(\Phi_b)$ to the measured ideality n; the equation holds for any dependence of $n(U,T)$ as well as for any U and T dependence of $\bar{\Phi}_b$ and σ_s.

In the following we restrict ourselves to the special case of voltage-*independent* idealities n, as our I/U data are well described by such a behavior. For such contacts a universal temperature dependence of the ideality n can be predicted from Eq. (21): According to Eqs. (17a) and (21), idealities n which are independent of bias U are only possible if both the mean barrier $\bar{\Phi}_b$ as well as the square of the standard deviation σ_s^2 vary *linearly* with bias U according to

$$\Delta\bar{\Phi}_b(U) = \bar{\Phi}_b(U) - \bar{\Phi}_{b0} = \rho_2 U, \tag{22a}$$

$$\Delta\sigma_s^2(U) = \sigma_s^2(U) - \sigma_{s0}^2 = \rho_3 U. \tag{22b}$$

The coefficients ρ_2 and ρ_3 (which may still depend on T) quantify the voltage deformation of the barrier distribution. If we hypothesize that a particular bias voltage U leads always to the *same change* of the barrier distribution with respect to zero bias (for example, by effects similar to image force lowering), then the coefficients ρ_2 and ρ_3 are independent of temperature T. Note that such an assumption does not require that the distribution under zero bias (i.e., $\bar{\Phi}_{b0}$ and σ_{s0}) itself be independent of T; we simply postulate that a specific bias U results in a specific change—*irrespective of* temperature T. Equating Eqs. (21), and (22a), and (22b) yields

$$n^{-1}(T) - 1 = -\rho_1(T) = -\rho_2 + \frac{\rho_3}{2kT/q}. \tag{23}$$

Equation (23) predicts a general temperature dependence of the ideality n of inhomogeneous Schottky contacts; the inverse ideality should be proportional to inverse temperature. A plot of $n^{-1}-1$ vs T^{-1} therefore should yield a straight line with an y-axis intercept and a slope which depend on the voltage coefficients ρ_2 and ρ_3.

Figure 8 is such a plot; it presents our idealities n for the two PtSi/Si samples. The idealities $n(T)$ from Fig. 4 change, indeed, in a manner which is anticipated on the basis of Eq. (23). The linear behavior in Fig. 8 proves that the ideality n in current/voltage curves of Schottky contacts represents the *voltage deformation* of the barrier distribution at the inhomogeneous interface. From the analysis of Fig. 8 we find the coefficients $\rho_2 = -0.034$ and $\rho_3 = -4.7$ mV for the PtSi/Si sample No. 1; the data of sample No. 2 yield $\rho_2 = -0.11$ and $\rho_3 = -5.3$ mV. We obtain the result $\rho_2 < 0$ and $\rho_3 < 0$ not only for the samples in Fig. 8, but also for other silicide/Si Schottky contacts. Table I demonstrates that this finding holds also if we evaluate the measured idealities of other authors. The increase of the current barrier Φ_b^j [(due to $n>1, \rho_1>0$), Eq. (18)] with increasing bias U is only possible because the decrease of the mean barrier $\bar{\Phi}_b$ (due to $\rho_2<0$) is compensated by a reduction of the value of σ_s (i.e., $\rho_3<0$): The application of a bias voltage obviously homogenizes the potential fluctuations; the higher the bias,

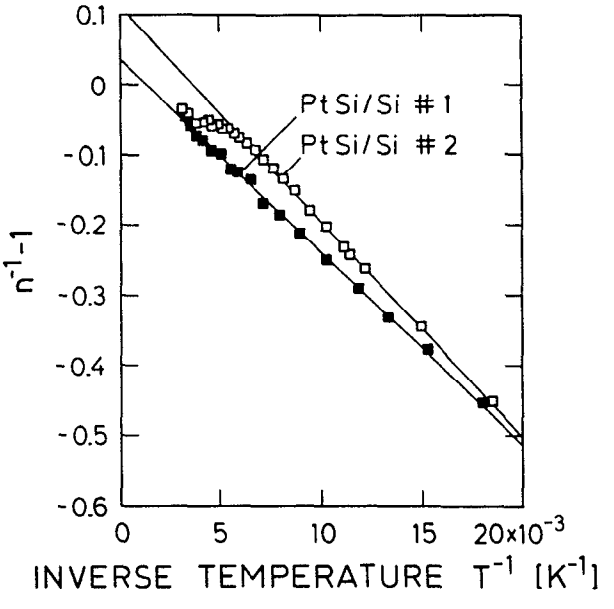

FIG. 8. The temperature-dependent ideality data of our PtSi/Si diodes follow Eq. (23). The linear behavior demonstrates that the ideality n indeed expresses the voltage deformation of the Gaussian distribution of Schottky barriers as proposed by our potential fluctuation model. The y-axis intercept and the slope of this plot yield the voltage coefficients ρ_2 and ρ_3. (For curve No. 2 only the linear part is used for the fit).

TABLE I. Voltage coefficients ρ_2 and ρ_3 as obtained by a fit of the temperature-dependent idealities in Fig. 9 to Eq. (23).

Contact	Ref.	ρ_2	ρ_3 (mV)	Curve No. in Fig. 9
Au/*n*-GaAs	34	−0.035	−8.2	7
Cr/*n*-Si	35	−0.013	−3.4	4
HP 2900	35	−0.003	−3.1	···
Ni/*n*-GaAs	36	−0.093	−9.6	6
Al/*n*-InP	37	−0.24	−15	8
Ti/*p*-Si	38	−0.08	−25	10
Al/*n*-GaAs	39	−0.043	−13	9
Ti/*n*-Si	40	−0.097	−4.8	1
Cu/*n*-Si	41	−0.096	−4.8	2
PtSi No. 1/*n*-Si		−0.034	−4.7	3
PtSi No. 2/*n*-Si		−0.11	−5.3	5

the narrower the barrier distribution $P(\Phi_b)$. The experimentally observed homogenization ($\rho_3 < 0$) of the barrier distribution under bias therefore also confirms our intuitive expectation which is based on the supposition that image forces shift the barrier maxima deeper into the semiconductor when the bias voltage increases.

E. Interpretation of $1/C^2$ plots

We also have to reinvestigate the significance of $1/C^2$ plots of measured capacitances C if we use them to deduce barrier data for inhomogeneous (and homogeneous) Schottky diodes with a voltage-dependent barrier Φ_b. From Eqs. (3a), (B5), and

$$\bar{\Phi}_b = \bar{V}_d + U + \zeta, \tag{24}$$

the voltage dependence of the areal capacitance C_F follows as

$$\frac{1}{C_F^2} = \frac{1}{\chi^2}\,[\bar{\Phi}_b(U) - U - \zeta - kT/q], \tag{25}$$

where χ was defined in Eq. (3a). Equation (25) shows that the $1/C^2$-vs-U plot remains linear even when the mean Schottky barrier $\bar{\Phi}_b$ depends linearly on voltage, as is found from the analysis of our I/U data. However, neither does the conventional analysis of the slope of such a plot yield the correct value for the doping N_d nor does the extrapolation toward the flatband voltage U_f give the correct zero-bias value of the mean barrier, i.e., $\bar{\Phi}_{b0}$. It is therefore fallacious to compare the capacitance barriers $\Phi_{b0}^{C'}$ in Fig. 4 [which are deduced from U_f and Eq. (3e)] with the zero-bias barriers Φ_{b0}^{j} from I/U curves. However, if we assume that the mean barrier $\bar{\Phi}_b$ shows under *reverse* bias the same linear voltage dependence as is determined from the analysis of the ideality n of the *forward*-bias I/U curve, then we can use the voltage coefficient ρ_2 which is determined with the help of the ideality data in Fig. 8. Inserting $\bar{\Phi}_b(U) = \bar{\Phi}_{b0} + \rho_2 U$ [from Eq. (22a)] into Eq. (25) yields then the correct mean zero-bias barrier

$$\bar{\Phi}_{b0} = U_f(1-\rho_2) + kT/q + \zeta, \tag{26a}$$

from the flatband voltage U_f. Since $\rho_2 < 0$, the values of the zero-bias capacitance barrier $\bar{\Phi}_{b0}$ from Eq. (26a) always exceed those from Eq. (3e). Similarly, the doping N_d which is determined by conventional analysis, without taking into account the voltage dependence of the mean barriers, will also come out too small. It follows from Eqs. (3a) and (25) that

$$\frac{d(C_F^{-2})}{dU} = \frac{-2(1-\rho_2)}{q\epsilon_s N_d}. \tag{26b}$$

The correct doping N_d is thus obtained by multiplying the value for N_d, which is obtained by a conventional analysis, i.e., from Eq. (3f), by the factor $(1-\rho_2)$. Because of the logarithmic dependence of ζ on N_d and the small value of ρ_2, this correction will only weakly influence $\bar{\Phi}_{b0}$.

Figures 4 and 7 show how the correction of the capacitance barriers affects our comparison of C/U and I/U barriers as well as the analysis of the standard deviation σ_s. Curves (b) and (d) in Fig. 7 present the differences $\bar{\Phi}_{b0} - \Phi_{b0}^{j}$ between the correct *zero-bias* barriers from both capacitance and current. It can be seen that the correction of the capacitance barriers shifts the curves only slightly upwards, but leaves the slopes essentially unchanged; the consideration of the voltage deformation of the barrier distribution is therefore not critical for the determination of the zero-bias standard deviation σ_{s0}. However, the apparent temperature dependence of the standard deviation of sample No. 1, which is expected from the uncorrected curve (a) is in fact removed [i.e., $\alpha_\sigma(1) = 0$], whereas the corrected curve (d) for sample No. 2 reveals a temperature dependence for σ_{s0} which follows Eq. (16a) with $\alpha_\sigma(2) = 11$ mV^2/K. From the analysis of the I/U and C/U measurements as well as of Fig. 8, we obtain then the following room-temperature results for our PtSi sample No. 1: $\Phi_{b0}^{j} = 837$ mV, $\Phi_{b0}^{C'} = 892$ mV, and $\Phi_{b0}^{C} = 914$ mV. The slope of curve (a) in Fig. 8 yields $\sigma_{s0} = 68.5$ mV; the corrected curve (c) yields $\sigma_{s0} = 69.3$ mV. For PtSi No. 2 we find $\Phi_{b0}^{j} = 848$ mV, $\Phi_{b0}^{C'} = 932$ mV, and $\Phi_{b0}^{C} = 1004$ mV. The slope of curve (b) in Fig. 8 yields $\sigma_{s0} = 68.9$ mV; the corrected curve (d) yields $\sigma_{s0} = 70.9$ mV.

V. EVALUATION OF PREVIOUSLY PUBLISHED DATA

A. Results

Here we show that not only our own measurements on PtSi/Si diodes, but also previously published data for Schottky contacts on Si, GaAs, and InP follow the linear dependence which is predicted by Eq. (23) and our model of potential fluctuations. Figure 9 presents data which are available for the measured temperature-dependent idealities $n(T)$ of abrupt Schottky contacts.[34–41] It can be seen that all data follow the predictions of Eq. (23); Table I compiles the corresponding voltage coefficients ρ_2 and ρ_3 which we obtain for $n(T)$.

All these earlier publications[34–41] used a one-dimensional band diagram as in Fig. 1 for the interpretation of measured data, and they did not give a conclusive explanation for $n(T)$. Some authors compensated the observed temperature dependence of the *barrier* $\Phi_{b0}^{j}(T)$ [as here obtained from the evaluation of Eqs. (1a) and (1b)] by introducing the ideality n also in the saturation current j_0 and expressed the current density j as

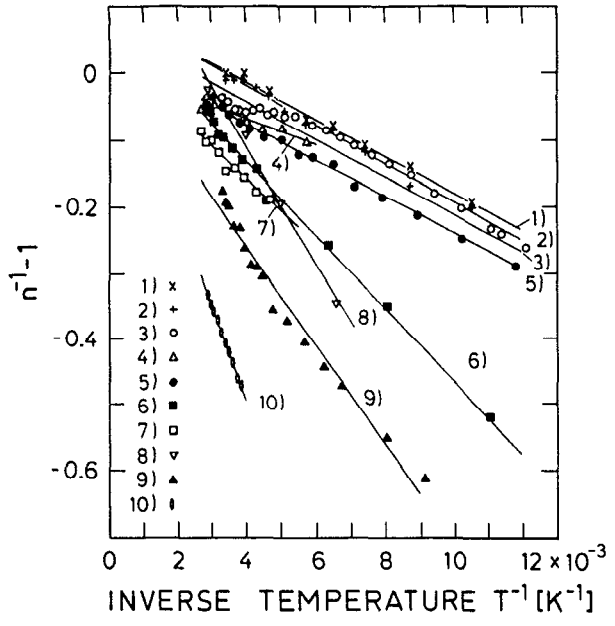

FIG. 9. All earlier measured temperature-dependent ideality data for abrupt Schottky contacts on GaAs (Refs. 34, 36, and 39), InP (Ref. 37), and Si (Refs. 35, 38, 40, and 41) follow also Eq. (23). References and voltage coefficients ρ_2 and ρ_3 are compiled in Table I.

$$j = A^{*}T^{2}e^{-q\Phi^{*}/(nkT)}(e^{qU/(nkT)}-1). \tag{27}$$

In some cases[35,37,40,41] it was then possible to obtain a straight line in the modified Richardson plot of the saturation value $\ln(j_0/T^2)$ vs $(nT)^{-1}$. Bhuiyan, Martinez, and Esteve used a similarly modified plot of $n(T)\ln(j_0/T^2)$ vs $1/T$.[39] Empirically, these authors[39] found also that the value of the capacitance barrier $\Phi_{b0}^{C'}$ could be approximately obtained if one multiplies the current barrier Φ^* from Eq. (27) by the ideality n; i.e., it holds that

$$\Phi_{b0}^{C'}(T) \approx n(T)\Phi^{*}. \tag{28}$$

However, all these publications[34-41] could not give satisfying physical explanations for the experimentally found $n(T)$ and the observations of straight lines in modified Richardson plots. In the next paragraph we discuss therefore how the temperature behavior of $n(T)$ is related to the so-called T_0 problem of Schottky diodes which is solved within the framework of our potential fluctuations model. The physical meaning of straight lines in the modified Richardson constant and the physical significance of Eq. (28) will be discussed in a further publication.[42]

B. Solution of the T_0 problem

Instead of using the ideality n as in Eq. (27), some authors[34-36,39,41] introduced a temperature T_0 and wrote the current as

$$j = A^{*}T^{2}e^{-q\Phi^{*}/k(T+T_0)}(e^{qU/k(T+T_0)}-1). \tag{29}$$

This is equivalent to requiring that the ideality n in Eq. (27) depend on temperature according to

$$n(T) = 1 + \frac{T_0}{T}. \tag{30}$$

Measured temperature-dependent ideality data for $T \gg T_0$ could be fitted with Eq. (30) and $T_0 = 50$ K for Au/GaAs (Ref. 34), $T_0 = 34$ K for Cr/Si (Ref. 35), $T_0 = 24$ K for HP diodes,[35] and $T_0 = 18$ K for Cu/n-Si.[41] In a thorough investigation Padovani showed that the T_0 values of Au/GaAs diodes which were fabricated on the same slice of GaAs can vary between 10 and 100 K.[43] Equation (30) and, as well, the values of T_0 were therefore solely empirically found and not based on theoretical arguments. In fact, Hackam and Harrop showed that Eq. (30) was inappropriate to describe their $n(T)$ data for Ni/GaAs diodes over the whole temperature range.[36] A temperature-*independent* $T_0 = 40 \pm 8$ K could only be used for the temperature range between 200 and 300 K.[36] In this regime their findings agreed with those of Padovani and Sumner.[34,36] However, for lower temperatures the value of T_0 increased up to 100 K, and measurements above 400 K could only be fitted by requiring even *negative* values for T_0.[36] This extreme example illustrates that Eq. (30) has no general validity to predict the temperature dependence of $n(T)$.

Levine[44] as well as Crowell[45] proposed to ascribe the necessity for introducing T_0 into the current/voltage curve Eq. (29) to either an exponential[44,45] or a parabolic[45] density of interface states. Unfortunately, both these models seem inappropriate to explain either the negative values[36] for T_0 or the temperature-dependent differences between the barriers from I/U and C/U data. On the other hand, capacitance and current barriers as well as *all* these published ideality data,[34-41] including those of Hackam and Harrop[36] (see curve 6 in Fig. 9), are well described by our model of potential fluctuations and Eq. (23).

The accidental success which was obtained in some cases in the past by fitting the temperature-dependent $n(T)$ with the empirical Eq. (30) instead of our Eq. (23) is based on the fact that Eq. (30) with the mysterious T_0 represents a coarse approximation to our Eq. (23): From Eq. (23) one obtains

$$n = \frac{1}{1-\rho_2+\rho_3/(2kT/q)}. \tag{31}$$

For the validity of

$$-\rho_2+\rho_3/(2kT/q) \ll 1, \tag{32}$$

Eq. (31) can be approximated by

$$n \approx 1+\rho_2-\frac{\rho_3}{2kT/q}. \tag{31'}$$

Table I shows that in most cases

$$\rho_2 \ll \rho_3/(2kT/q) \ll 1 \tag{32'}$$

holds, and as a second approximation to Eqs. (23) and (31), one may indeed write

$$n \approx 1-\frac{\rho_3}{2kT/q} \equiv 1+\frac{T_0}{T}. \tag{31''}$$

Equating Eqs. (30) and (31'') thus yields

$$T_0 \approx -\frac{\rho_3}{2k/q}. \tag{33}$$

We reveal therefore the physical meaning of the puzzling T_0

as the temperature equivalent of the coefficient ρ_3 which describes the narrowing of the Gaussian barrier distribution upon the application of a bias voltage. Vice versa, the coefficient ρ_3 represents the voltage equivalent of T_0. If we use our ρ_3 values from Table I and calculate T_0 with the help of Eq. (33), then the results are close to the above-cited literature values for T_0. We understand also why the $n(T)$ data could approximately be fitted with Eq. (30) under the condition $T_0 \ll T$: The requirement $T_0 \ll T$ is equivalent to the second part of Eq. (32') which must be valid to approximate Eqs. (23) and (31) by Eq. (31").

VI. CONCLUSIONS

Our investigations have shown that spatial inhomogeneities of the barrier and band bending at Schottky contacts strongly affect the transport at such interfaces. We have presented here a new model of potential fluctuations that quantitatively explains the different barriers from capacitance and current measurements: Capacitances depend only on the mean value $\overline{\Phi}_b$ of the barrier distribution $P(\Phi_b)$, whereas current barriers Φ_b^j are lower by a value which depends on the standard deviation σ_s of the distribution and is given by Eq. (14). Our model explains the observed temperature-dependent differences of capacitance and current barriers which are not explained by other conventional and one-dimensional Schottky contact theories. We have here proposed to use a plot of the zero-bias values $\overline{\Phi}_{b0} - \Phi_{b0}^j$ versus inverse temperature to determine the zero-bias standard deviation σ_{s0}. For our PtSi/Si diodes we find typical σ_{s0} values around 70 mV, which are seemingly small when compared to the mean values of room-temperature values $\overline{\Phi}_{b0} \approx 920$ mV; nevertheless, these small potential fluctuations drastically affect low-temperature I/U data. In particular, they are responsible for the curved behavior of Richardson plots as in Fig. 3.

Idealities $n > 1$ of Schottky contacts have been shown here to result from the deformation of the barrier distribution $P(\Phi_b)$ when a bias voltage is applied. For Schottky contacts with voltage-*independent* idealities n in I/U curves, the mean barriers $\overline{\Phi}_b$ as well as the square of the standard deviation of the barrier distribution σ_s^2 depend linearly on bias voltage. The voltage coefficients ρ_2 and ρ_3 of $\overline{\Phi}_b$ and σ_s^2 can be deduced with the help of a new analysis which uses a plot based on Eq. (23). Measured voltage-*independent* idealities n of I/U curves can also be used for an improved evaluation of conventional $1/C^2$ plots of inhomogeneous Schottky contacts.

Our potential fluctuations model offers also a solution to the long-standing T_0 problem of Schottky contacts. We have demonstrated that under certain approximations, as described by Eqs. (31) and (32), the mysterious T_0 represents the temperature equivalent of the voltage coefficient ρ_3 which describes the narrowing of the Gaussian barrier distribution upon the application of bias voltages.

Finally, we want to emphasize that current/voltage measurements at room temperature are by no means sufficient to demonstrate spatially homogeneous Schottky contacts—even when the ideality n is close to unity. On the contrary, reliable characterizations of Schottky diodes require capacitance *and* current measurements over a wide temperature range. It seems therefore also not appropriate to deduce temperature coefficients of current barriers $\Phi_{b0}^j(T)$ from I/U measurements alone if one intends to compare the results with theories[32] which predict the temperature coefficients of fundamental (mean) Schottky barriers. At last, we note that our analysis seems appropriate to characterize the electronic homogeneity not only of polycrystalline, but also of single-crystalline, epitaxial Schottky diodes.

ACKNOWLEDGMENTS

The authors gratefully acknowledge the generous and continuous support and encouragement of H. J. Queisser. We thank him also for a critical reading of the manuscript. This work is supported by the German Ministry for Research and Technology under Contract No. 0328962A.

APPENDIX A

The band bending V_d^j which is effective for the current j across the Schottky contact is calculated from

$$e^{-qV_d^j/kT} = \int_{-\infty}^{\infty} e^{-qV_d/kT} P(V_d)\,dV_d. \tag{A1}$$

If we scale all quantities with the thermal voltage kT/q according to

$$u_s = q(V_d - \overline{V}_d)/kT, \tag{A2}$$

$$\sigma_T = q\sigma_s/kT, \tag{A3}$$

$$V_{d,T}^j = qV_d^j/kT, \tag{A4}$$

$$\overline{V}_{d,T} = q\overline{V}_d/kT, \tag{A5}$$

we find

$$e^{-V_{d,T}^j} = e^{-\overline{V}_{d,T}} \frac{1}{\sigma_T\sqrt{2\pi}} \int_{-\infty}^{\infty} e^{-u_s} e^{-u_s^2/(2\sigma_T^2)}\,du_s. \tag{A6}$$

The value of the integral is[31] $\sigma_T(2\pi)^{1/2}\exp(\sigma_T^2/2)$, which yields the result

$$V_{d,T}^j = \overline{V}_{d,T} - \sigma_T^2/2. \tag{A7}$$

From Eq. (A7) one then obtains Eq. (12).

APPENDIX B

According to Eq. (3a), the areal capacitance $C_F = C/F_C$ is equal to $C_F(V_d) = \chi(V_d - kT/q)^{-1/2}$. For a distribution of potentials, one gets, for the integrated areal capacitance with an effective capacitance band bending V_d^C,

$$C_F(V_d^C) = \chi \frac{1}{\sigma_s\sqrt{2\pi}} \int_{-\infty}^{\infty} \frac{1}{\sqrt{V_d - kT/q}} P(V_d)\,dV_d \tag{B1}$$

$$= \chi \frac{1}{\sigma_T\sqrt{2\pi}} \frac{1}{\sqrt{kT/q}} \int_{-\infty}^{\infty} \frac{1}{\sqrt{\overline{V}_{d,T} + u_s - 1}} \times e^{-u_s^2/(2\sigma_T^2)}\,du_s \tag{B2}$$

$$= C_F(\overline{V}_d) \frac{1}{\sigma_T\sqrt{2\pi}} \int_{-\infty}^{\infty} \frac{1}{\sqrt{1 + u_s/(\overline{V}_{d,T-1})}} \times e^{-u_s^2/(2\sigma_T^2)}\,du_s. \tag{B3}$$

For $u_s \gg V_{d,T}$, which is equivalent to $V_d \gg kT/q$ (the validity range of the depletion approximation), we can expand the root under the integral into a series and then obtain

$$C_F(V_d^C) = C_F(\overline{V}_d)\left(\frac{1}{\sigma_T\sqrt{2\pi}}\int_{-\infty}^{\infty} e^{-u_s^2/(2\sigma_T^2)}du_s - \frac{1/(2\overline{V}_{d,T})}{\sigma_T\sqrt{2\pi}}\int_{-\infty}^{\infty} u_s e^{-u_s^2/(2\sigma_T^2)}du_s\right). \tag{B4}$$

The first part in the large parentheses yields unity (normalization of the Gaussian distribution), whereas the second integral equals zero [the expectation value of the Gaussian distribution $P(u_s)$]; thus we get the result for the integrated areal capacitance:

$$C_F(V_d^C) = C_F(\overline{V}_d) = \sqrt{\frac{q\epsilon_s N_d/2}{\overline{V}_d - kT/q}}, \tag{B5}$$

i.e., $V_d^C = \overline{V}_d$.

Note added in proof: Recently we found that temperature-dependent barrier measurements were also discussed by Singh, Reinhardt, and Anderson[46] as well as by Song *et al.*[47]

[1] S. M. Sze, *Physics of Semiconductor Devices*, 2nd ed. (Wiley, New York, 1981), Chaps. 5 and 6.
[2] E. H. Rhoderick and R. H. Williams, *Metals Semiconductor Contacts*, 2nd ed. (Clarendon, Oxford, 1988), Chaps. 3 and 4.
[3] J. H. Werner, Appl. Phys. A **47**, 291 (1988).
[4] For a critical review on interface states measurements and the influence of minority carriers on current transport at Schottky contacts, see J. H. Werner, in *Metallization and Metal-Semiconductor Interfaces*, edited by I. P. Batra (Plenum, New York, 1989), p. 235.
[5] H. C. Card and E. H. Rhoderick, J. Phys. D **4**, 1589 (1971).
[6] J. H. Werner, K. Ploog, and H. J. Queisser, Phys. Rev. Lett. **57**, 1080 (1986).
[7] J. H. Werner, A. F. J. Levi, R. T. Tung, M. Anzlowar, and M. Pinto, Phys. Rev. Lett. **60**, 53 (1988).
[8] See E. H. Rhoderick and R. H. Williams, *Metal Semiconductor Contacts*, 2nd ed. (Clarendon, Oxford, 1988), p. 113; see also R. F. Broom, H. P. Meier, and W. Walter, J. Appl. Phys. **60**, 1833 (1986).
[9] V. L. Rideout and C. R. Crowell, Solid-State Electron. **13**, 993 (1970).
[10] See E. H. Rhoderick and R. H. Williams, *Metal Semiconductor Contacts*, 2nd ed. (Clarendon, Oxford, 1988), p. 118; see also C. T. Sah, R. N. Noyce, and W. Shockley, Proc. IRE **45**, 1228 (1957).
[11] H. H. Güttler and J. H. Werner, Appl. Phys. Lett. **56**, 1113 (1990).
[12] A. J. Madenach and J. H. Werner, Phys. Rev. Lett. **55**, 1212 (1985); Phys. Rev. B **38**, 13 150 (1988).
[13] J. M. Andrews and M. P. Lepselter, Solid-State Electron. **13**, 1011 (1970).
[14] F. A. Padovani and R. Stratton, Solid-State Electron. **9**, 695 (1966).
[15] C. Y. Chang and S. M. Sze, Solid-State Electron. **13**, 727 (1970).
[16] See E. H. Rhoderick and R. H. Williams, *Metal Semiconductor Contacts*, 2nd ed. (Clarendon, Oxford, 1988), pp. 99 and 100.
[17] A. B. McLean, I. M. Dharmadasa, and R. H. Williams, Semicond. Sci. Technol. **1**, 137 (1986).
[18] D. Arnold and K. Hess, J. Appl. Phys. **61**, 5178 (1987).
[19] J. A. Nixon and J. H. Davies, Phys. Rev. B **41**, 7929 (1990).
[20] I. Ohdomari, T. S. Kuan, and K. N. Tu, J. Appl. Phys. **50**, 7020 (1979).
[21] I. Ohdomari and K. N. Tu, J. Appl. Phys. **51**, 3735 (1980).
[22] R. D. Thompson and K. N. Tu, J. Appl. Phys. **53**, 4285 (1982).
[23] T. Okumura and K. N. Tu, J. Appl. Phys. **54**, 922 (1983).
[24] M. V. Schneider, A. Y. Cho, E. Kollberg, and H. Zirath, Appl. Phys. Lett. **43**, 558 (1983).
[25] T. Q. Tuy and I. Mojzes, Appl. Phys. Lett. **56**, 1652 (1990).
[26] J. L. Freeouf, T. N. Jackson, S. E. Laux, and J. M. Woodall, Appl. Phys. Lett. **40**, 634 (1982); J. Vac. Sci. Technol. **21**, 570 (1982).
[27] J. Werner and H. Strunk, J. Phys. (Paris) Colloq. **44**, C1-99 (1983).
[28] J. H. Werner, thesis, University of Stuttgart, 1983 (unpublished); see also J. H. Werner, in *Polycrystalline Semiconductors—Physical Properties and Applications*, edited by G. Harbeke (Springer, Berlin, 1985), p. 76.
[29] D. J. Thomson and H. C. Card, J. Appl. Phys. **54**, 1976 (1983).
[30] G. D. Mahan, J. Appl. Phys. **55**, 980 (1984).
[31] W. Gröbner and N. Hofreiter, *Bestimmte Integrale* (Springer, Berlin, 1966), p. 65W.
[32] M. Cardona and N. E. Christensen, Phys. Rev. B **35**, 6182 (1987); M. Cardona and S. Gopalan, in *Progress in Electron Properties of Solids*, edited by E. Doni, R. Girlanda, G. Pastori Parravicini, and A. Quattropani (Kluwer Academic, Rome, 1989), pp. 51–64.
[33] A direct comparison would be possible on the basis of *absolute* values of I and C if the doping N_d was exactly known within a few percent.
[34] F. A. Padovani and G. G. Sumner, J. Appl. Phys. **36**, 3744 (1965).
[35] N. Saxena, Surf. Sci. **13**, 151 (1969).
[36] R. Hackam and P. Harrop, IEEE Trans. Electron Devices **ED-19**, 1231 (1972).
[37] B. Tuck, G. Eftekhari, and D. M. de Cogan, J. Phys. D **15**, 457 (1982).
[38] P. L. Hanselaer, W. H. Laflère, R. L. Van Meirhaeghe, and F. Cardon, J. Appl. Phys. **56**, 2309 (1984).
[39] A. S. Bhuiyan, A. Martinez, and D. Esteve, Thin Solid Films **161**, 93 (1988).
[40] M. O. Aboelfotoh, Phys. Rev. B **39**, 5070 (1989), Fig. 5.
[41] M. O. Aboelfotoh, A. Cros, B. G. Svensson, and K. N. Tu, Phys. Rev. B **41**, 9819 (1990), Fig. 3.
[42] J. H. Werner and H. H. Güttler (unpublished)
[43] F. A. Padovani, in *Semiconductors and Semimetals*, edited by R. K. Willardsen and A. C. Beer (Academic, New York, 1971), Vol. 7 A, Chap. 2.
[44] J. D. Levine, J. Appl. Phys. **42**, 3991 (1971).
[45] C. R. Crowell, Solid-State Electron. **20**, 171 (1977).
[46] A. Singh, K. C. Reinhardt, and W. A. Anderson, J. Appl. Phys. **68**, 3475 (1990).
[47] Y. P. Song, R. L. van Meirhaeghe, W. H. Laflère, and F. Cardon, Solid-State Electron. **29**, 633 (1986).